PNAS
www.pnas.org

Supplementary Information for

Dopaminergic basis for signaling belief updates, but not surprise, and the link to paranoia

Matthew M Nour, Tarik Dahoun, Philipp Schwartenbeck, Rick A Adams, Thomas HB FitzGerald, Christopher Coello, Matthew B Wall, Raymond J Dolan, Oliver D Howes

Corresponding Authors

Dr Matthew Nour, matthew.nour@kcl.ac.uk

PO63 Level 5, IOPPN, King's College London, 16 De Crespigny Park, London SE5 8AF

Professor Oliver Howes, oliver.howes@kcl.ac.uk

PO63 Level 5, IOPPN, King's College London, 16 De Crespigny Park, London SE5 8AF

This PDF file includes:

www.pnas.org/cgi/doi/10.1073/pnas.1809298115

SUPPLEMENTARY MATERIALS AND METHODS

Subjects

The study was conducted at Imanova Centre for Imaging Sciences, London. 41 healthy volunteer subjects were initially recruited through local media and university advertisements. Subjects had no history of neuropsychiatric disorder, a negative urine drug screen prior to scanning, and provided written informed consent to take part in the experiment. Two subjects were excluded from fMRI analysis. One subject did not receive adequate training in the task prior to scanning owing to technical problems, and a second was unable to perform the task beyond chance level (correlation between subject performance and that of an 'ideal Bayesian observer' was r = .04, and this subject was the only one for whom this measure of performance was more than 3 standard deviations less than the group mean). Thirty-nine subjects were therefore included in the fMRI analysis.

Task Details

The task and training procedures were identical to a previously published study.[1] During training, subjects were familiarized with two visual and two auditory cues, and learned that for each sensory modality (visual and auditory) one cue could be considered 'good' (in that it predicted monetary gains with approx. 90% validity) and one was 'bad' (in that it predicted monetary losses with approx. 90% validity). Subjects were informed (correctly) that these identities would remain stable throughout the experiment. Training also familiarized subjects with the task structure (state transition probabilities and cue validity).

In the task itself, for any given trial subjects were simultaneously presented with one visual and one auditory cue, followed by a monetary outcome (gains or losses from 10-30p). They were informed that for any given trial only one cue modality (visual or auditory) was relevant for predicting the monetary outcome, and that the identity of the relevant (predictive) cue modality would remain stable for a short period of time, but would periodically switch (5-6 times) in a session of 60 trials. The goal of the task was to correctly track the identity of the relevant cue modality (i.e. the current task state) at each trial, using information from cue-outcome observations. At the end of each trial participants reported their belief regarding the current informative modality using an 11-point rating bar.

For each trial, cues were presented for 2 s, followed by a gap jittered between 2 and 8 s. The monetary outcome was then shown for 2 s. Subsequently, a rating bar appeared for 4 s, at which time subjects indicated their beliefs about the relevant (predictive) cue modality using an MRI-compatible button box, by moving a cursor on the rating bar from 1 (left extreme, indicating complete certainty that one cue modality was relevant) to 11 (right extreme, indicating complete certainty that the other cue modality was relevant). The identities of the left and right extremes of the rating bar were alternated for each session, and the cursor

was positioned randomly at either the left or right extreme of the rating bar at the appearance of the rating bar on each trial. The next trial started after an inter-trial interval (fixation cross) jittered between 1 and 3 s.

Subjects' ratings at the end of each trial were assumed to result from their belief about the relevant modality before seeing the monetary outcome (prior belief), and their estimation of the likelihood of the observed cue-outcome pairing under the two competing hypotheses about the identity of the task-relevant modality. Importantly, in half of the trials the visual and auditory cue had the same valence (i.e. both were 'good' or both were 'bad'). The monetary outcome of these trials was therefore not informative about the identity of the relevant cue modality. Crucially, however, 'noninformative' trials could still lead to an unexpected (surprising) observation in the (approximately 10% of) trials where the monetary outcome was improbable under both auditory and visual cues (leading to positive information-theoretic surprise, but zero Bayesian surprise). The remaining trials were 'informative', in that the visual and auditory cues predicted different outcomes. On these trials the observed monetary outcome would differentially favour one hypothesis about the relevant modality more than the other. Unexpected observations on these trials (i.e. monetary outcomes that were improbable under the participant's prior belief about the relevant modality) indicated a potential switch in the relevant modality. These observations were therefore associated with both positive information theoretic surprise and positive Bayesian surprise. Thus, the task de-correlated information-theoretic and Bayesian surprise. Mean winnings in the 39 subjects across 3 sessions of the fMRI task were £24.30 (SD £3.68).

Computational Modelling

To capture behaviour we used a simple Hidden Markov Model (HMM), identical to that used in a previous study using this task.[1]

Here, across a session of length T trials, the system moves though hidden states $x_{1:T} \in \{1,2\}$ ('auditory cues relevant' corresponds to $x_t = 1$, 'visual cues relevant' corresponds to $x_t = 2$), which must be inferred from monetary outcomes $y_{1:T} \in \{1,2\}$ (wins correspond to $y_t = 1$, and losses to $y_t = 2$), auditory cues $a_{1:T} \in \{1,2\}$, and visual cues $v_{1:T} \in \{1,2\}$ (win-predicting 'good' cues correspond to $a_t = 1$ and $v_t = 1$, and loss-predicting 'bad' cues to to $a_t = 2$ and $v_t = 2$), all of which are directly observed (*t* indicates the current trial). For clarity of notation, we additionally define $o_t = [y_t\ a_t\ v_t]$ as the specific combination of monetary outcome, auditory and visual cues observed on each trial. Transition probabilities between hidden states are encoded in a 2 x 2 matrix $\mathbf{B}$ such that

$$\mathbf{B} = \begin{bmatrix} \delta & 1-\delta \\ 1-\delta & \delta \end{bmatrix} \qquad \textbf{Eq. 1}$$

$$p(x_t = j|x_{t-1} = i) = b_{ij} \quad \textbf{Eq. 2}$$

where $1 - \delta$ specifies the probability of a switch (reversal) between states (i.e. a change in the identity of the relevant modality). Observation probabilities under each state were encoded in a 2 x 2 matrix $\mathbf{A}$ where

$$\mathbf{A} = \begin{bmatrix} \psi & 1-\psi \\ 1-\psi & \psi \end{bmatrix} \quad \textbf{Eq. 3}$$

$$p(o_t = [i\ j\ k]|x_t = 1) = a_{ij} \quad \textbf{Eq. 4}$$

$$p(o_t = [i\ j\ k]|x_t = 2) = a_{ik} \quad \textbf{Eq. 5}$$

Here, the cue validity parameter ψ governs how reliably the relevant cue modality predicts the monetary outcome. Thus, good cues (of the relevant modality) predict a win with probability ψ, and a loss with probability $1 - \psi$, and bad cues the converse. Initial state probabilities $p(x_1)$ are assumed to be uniform.

Given the conditional independence properties of the HMM, trial-by-trial belief updating can be performed by iterative applications of Bayes rule:

$$p(x_t|o_{1:t}, \mathbf{A}, \mathbf{B}) = \frac{p(o_t|x_t, \mathbf{A}, \mathbf{B})p(x_t|o_{1:t-1}, \mathbf{A}, \mathbf{B})}{p(o_t|o_{1:t-1}, \mathbf{A}, \mathbf{B})} \quad \textbf{Eq. 6}$$

, where for all trials *t>1*, a subject's posterior belief about the task-relevant modality after observing the cue-outcome pair, $p(x_t|o_{1:t}, \mathbf{A}, \mathbf{B})$, is proportional to the product of their estimate of the likelihood of observing the cue-outcome pair under each hypothesis, $p(o_t|x_t, \mathbf{A}, \mathbf{B})$ (captured by the free parameter ψ) and their prior belief about the task-relevant modality, $p(x_t|o_{1:t-1}, \mathbf{A}, \mathbf{B})$. The prior belief is dependent on the posterior belief from the previous trial, $p(x_{t-1}|o_{1:t-1}, \mathbf{A}, \mathbf{B})$, and the participant's belief about the probability of states remaining stable from one trial to the next, $p(x_t|x_{t-1}, \mathbf{A}, \mathbf{B})$, captured by the free parameter δ.

$$p(x_t|o_{1:t-1}, \mathbf{A}, \mathbf{B}) = p(x_t|x_{t-1}, \mathbf{A}, \mathbf{B})\ p(x_{t-1}|o_{1:t-1}, \mathbf{A}, \mathbf{B}). \quad \textbf{Eq. 7}$$

For brevity we ignore the dependence on model m, but this is implied.

We estimated the two free parameters (ψ and δ) using constrained maximum-likelihood estimation (both parameters constrained between 0.5 and 1.0, inclusive). To identify optimal parameter settings for each subject, the fitting algorithm (instantiated in the Matlab-routine *fmincon*) was specified to maximize the

explained variance (R^2) in a linear model in which observed behaviour (belief rating about relevant cue modality) was predicted by the Bayesian model's predicted belief about the relevant modality.

For our subsequent imaging analysis (both GLM1 and GLM2), we defined the following trial-by-trial regressors based on the fitted model for each subject:

$$\alpha_t = D_{KL}\big(p(x_t|o_{1:t}, \mathbf{A}, \mathbf{B}) \,||\, p(x_t|o_{1:t-1}, \mathbf{A}, \mathbf{B})\big) \qquad \textbf{Eq. 8}$$
$$= \sum_{i=1}^{2} (p(x_t = i|o_{1:t}, \mathbf{A}, \mathbf{B}) \ln \frac{p(x_t = i|o_{1:t}, \mathbf{A}, \mathbf{B})}{p(x_t = i|o_{1:t-1}, \mathbf{A}, \mathbf{B})})$$

corresponding to the Bayesian surprise (D_{KL} from prior to posterior beliefs at each trial), and

$$\beta_t = -\ln p(o_t|o_{1:t-1}, \mathbf{A}, \mathbf{B}) \qquad \textbf{Eq. 9}$$
$$= -\ln \sum_{i=1}^{2} \big(p(o_t|x_t = i, \mathbf{A}, \mathbf{B}) p(x_t = i|o_{1:t-1}, \mathbf{A}, \mathbf{B})\big),$$

corresponding to the information-theoretic surprise (I_S) of an observation, given the prior belief. For GLM2 we also defined the entropy over prior beliefs at cue presentation ('model-derived uncertainty') as the following:

$$H_t = -\sum_{i=1}^{2} (p(x_t = i|o_{1:t-1}, \mathbf{A}, \mathbf{B}) \ln p(x_t = i|o_{1:t-1}, \mathbf{A}, \mathbf{B})) \qquad \textbf{Eq. 10}$$

MR Image Acquisition and Analysis

MR images were acquired using a Siemens MAGNETOM Verio 3-T MR scanner and a 32-channel phased-array head-coil. We acquired one high-resolution T1-weighted structural volume for the purpose of fMRI and PET coregistration, and B0 fieldmaps in order to unwarp EPI images during spatial pre-processing. The T1-weighted volume was acquired using a Magnetization Prepared Rapid Gradient Echo (MPRAGE) sequence using parameters from the Alzheimer's Disease Research Network (ADNI-GO; 160 slices x 240 x 256, TR = 2300 ms, TE = 2.98 ms, flip angle = 9°, 1 mm isotropic voxels, bandwidth = 240Hz/pixel, parallel imaging (PI) factor =2).[2] B0 fieldmaps were acquired using a dual-echo gradient-echo sequence (TR = 599 ms, TE 1 = 5.19 ms, TE 2 = 7.65 ms, flip angle = 60°, 3 mm isotropic voxels, 55 axial slices, bandwidth = 260 Hz/pixel).

Each scanning session started with a 'sound test' to ensure that subjects could distinguish the task auditory cues confidently against background scanner noise. Foam head-restraint pads were used to minimize head

movement. Respiratory and cardiac activities were measured using a respiration band and finger pulse oximeter to allow for physiological noise correction in the imaging analysis.[3]

During pre-processing, fMRI time series were realigned to the mean image and unwarped using the B0 fieldmaps generated by the Fieldmap toolbox.[4] Image normalization to MNI space was accomplished using the DARTEL toolbox,[5] with 6mm full-width at half-maximum (FWHM) Gaussian kernel smoothing.

For the first level general linear model (GLM) described in the main text, we used model-derived participant-specific estimates for Bayesian surprise and information-theoretic surprise as the trial-by-trial regressors of interest at outcome presentation. This means that we can have a high degree of confidence that the resulting fMRI findings are closely related to individual participant belief updating behaviour. The pairwise correlations between the parametric regressors at outcome presentation are shown in **SI Appendix Table S6** and are numerically similar to those reported in a previous study using the same model.[1] As nuisance regressors, first level GLMs included 6 realignment parameters and 18 physiological noise parameters, derived via RETROICOR using Fourier expansions for the estimated phases of cardiac pulsation, respiration and cardio-respiratory interactions (3^{rd}, 4^{th} and 1^{st} order, respectively),[6–8] implemented in the PhysIO toolbox (https://www.tnu.ethz.ch/en/home.html[3]). Temporal derivatives were included to account for slice-timing effects. An AR(1) model was used to account for serial autocorrelations, and we applied a 128s high-pass filter.

In addition to the GLM used in the main analysis (referred to as GLM1, and outlined in the main text), we conducted a second analysis (GLM2) in which the 'subjective uncertainty' parametric regressor at cue onset was replaced with an estimate of entropy over prior beliefs derived from the participant-specific fitted model ('model-derived uncertainty', H, **SI Appendix Eq. 10**). The correlation between subjective uncertainty (in GLM1) and model-derived uncertainty (in GLM2) across all subjects was r = .46 [.39, .52]. Results from GLM2 are only reported for the analysis of belief uncertainty at cue onset (in comparison with GLM1), however all GLM2 results for neural encoding of Bayesian and information-theoretic surprise, and the significant PET-fMRI correlations, are quantitatively similar to those from GLM1. One additional participant was excluded from the GLM2 analysis, as the behavioural responses of this participant resulted in a rank deficient design matrix ($\delta = 0.5$ in participant number 23, resulting in a uniform H).

fMRI activation maps are displayed as overlays on the SPM default 152-subject T1-weighted average volume. Projections onto the inflated cortical surface are created using bspmview (http://www.bobspunt.com/bspmview/).

PET Image Acquisition and Analysis

Prior to injection of the radiotracer and starting the PET acquisition, each subject first received a low-dose computed tomography scan for attenuation and model-based scatter correction. Dynamic PET images were reconstructed using a filtered back-projection algorithm into 31 frames (8 x 15 seconds, 3 x 60 seconds, 5 x 120 seconds, 15 x 300 seconds) with a 128 matrix, a zoom of 2.6 and a transaxial Gaussian filter of 5mm.

Structural MR images were segmented using SPM functions to obtain grey matter masks used for the definition of the reference region during the kinetic analysis. The ICBM152 template was non-linearly warped to each subject's structural MRI, and the derived deformation parameters were applied to our neuroanatomical atlas, to obtain a parcellation of each subject's brain into the studied ROIs (bilateral whole striatum[9] and SN/VTA[1,10]). The MRI, associated individual parcellation and associated grey matter masks were then downsampled to the PET resolution (2mm). Dynamic PET images were corrected for motion using a frame-by-frame registration process with a mutual information cost function. For each subject the averaged PET image from the entire scan duration was registered to the downsampled structural MRI scan with rigid-body registration. The rigid body matrix was subsequently applied to the motion corrected dynamic PET. Regional time activity curves (TAC) were obtained by applying the downsampled individual anatomical parcellations to the motion corrected dynamic PET image.

The non-displaceable binding potential (BP_{ND}) of [^{11}C]-(+)-PHNO is defined as follows:

$$BP_{ND} = \frac{f_{ND} B_{max}(1-\sigma)}{K_D} \qquad \textbf{Eq. 11}$$

where f_{ND} the non-displaceable free fraction of PHNO in the brain, B_{max} is the total D2/3R density, σ is the fraction of receptors bound by endogenous dopamine, and $1/K_D$ is the affinity of radioligand for the target. The simplified reference tissue model (SRTM) was used to derive BP_{ND} from the regional TACs.[11,12] We used cerebellar grey matter as the reference region, defined as the intersection of the warped cerebellum atlas[13] and individual subject grey matter mask.

The magnitude of dexamphetamine-induced dopamine release for each subject was quantified as the percentage reduction in BP_{ND} in the dexamphetamine condition compared to the baseline (no dexamphetamine) condition.

$$\Delta\, BP_{ND} = 100 \cdot \frac{BP_{ND\,(baseline)} - BP_{ND\,(dexamphetamine)}}{BP_{ND\,(baseline)}}\% \qquad \textbf{Eq. 12}$$

Statistical Analysis

Whole brain PET-fMRI analysis

In addition to ROI-level PET-fMRI correlations, we also investigated the PET-fMRI relationships of interest in a series of second level whole brain fMRI analyses. Specifically, we conducted two regression analysis on the estimated responses for Bayesian surprise from the first-level analysis. The first regression model included midbrain BP_{ND} as a regressor, and the second included whole striatum $\Delta\, BP_{ND}$ as a regressor. We then repeated this procedure on the estimated responses for information-theoretic surprise from the first-level analysis. In all four models we tested the negative linear relationship between fMRI and PET measures across all voxels showing group level significant activation for the original fMRI contrast (Bayesian or information-theoretic surprise) at whole brain cluster level. We used identical criteria for establishing statistical significance in these whole brain fMRI-PET analyses as in the fMRI activation analysis (i.e. $P < 0.05$, family-wise error corrected either at whole brain cluster level or using a small volume correction with the SN/VTA and ventral striatum ROI).

Behaviour-PET Statistical Analysis

Based on the existing literature we hypothesised that there would be an inverted-U relationship between the ability to flexibility update internal representations (measured as trial-by-trial behavioural sensitivity to meaningful information, i.e. the mean difference in reported belief update between informative and non-informative trials) and baseline D2/3R signalling in the striatum (indexed by the fraction of total D2/3Rs under tonic stimulation by endogenous dopamine, σ).[14] Striatal [^{11}C]-(+)-PHNO BP_{ND} is sensitive to inter-individual differences in synaptic dopamine concentration,[15,16] such that it is proportional not only to the total density of D2/3Rs (B_{max}), but also to the fraction of available D2/3Rs that are *not* bound by endogenous dopamine $(1-\sigma)$ (see **SI Appendix Eq. 11**).[15] If cognitive flexibility shows an inverted-U relationship with the fraction of D2/3Rs tonically occupied by endogenous dopamine (σ), then it can be shown algebraically that cognitive flexibility will also show an inverted-U relationship with BP_{ND}.

Throughout, we consider $P < 0.05$ as statistically significant. All statistical analyses were conducted using MATLAB Version 2015b.

SUPPLEMENTARY RESULTS

Behavioural Analysis

As outlined in the primary results, poor overall performance was positively correlated with the absolute magnitude of reported belief shifts on non-informative trials. This might reflect a tendency to increase belief uncertainty on non-informative trials (i.e. moving from one extremity of the rating bar, towards the middle indifference point, which may be adaptive), or a tendency to switch belief about the relevant modality from one hypothesis to a competing hypothesis (i.e. moving from one extremity of the rating bar to the other extremity, which is always maladaptive for non-informative trials). In support of the latter hypothesis, belief shifts on non-informative trials directly correlated with the mean number of times participants changed their belief about the relevant modality from one hypothesis to a competing hypothesis (termed a 'belief switch') on these trials (rho = .72 [.52, .85], $P < 0.001$), but not with mean increase in reported belief uncertainty (rho = .21 [-.12, .50], $P = 0.20$). Moreover, overall behavioural performance was negatively related to the mean number of belief switches in non-informative trials (rho = -.63 [-.79, -.38], $P < 0.001$), but not informative trials (rho = -.19 [-.49, .14], $P = 0.24$). In line with our findings that paranoia is related to maladaptive task performance, there was a positive correlation between paranoia and belief switches on non-informative trials (rho = .43 [.13, .66], $P = 0.006$).

Fig. S1

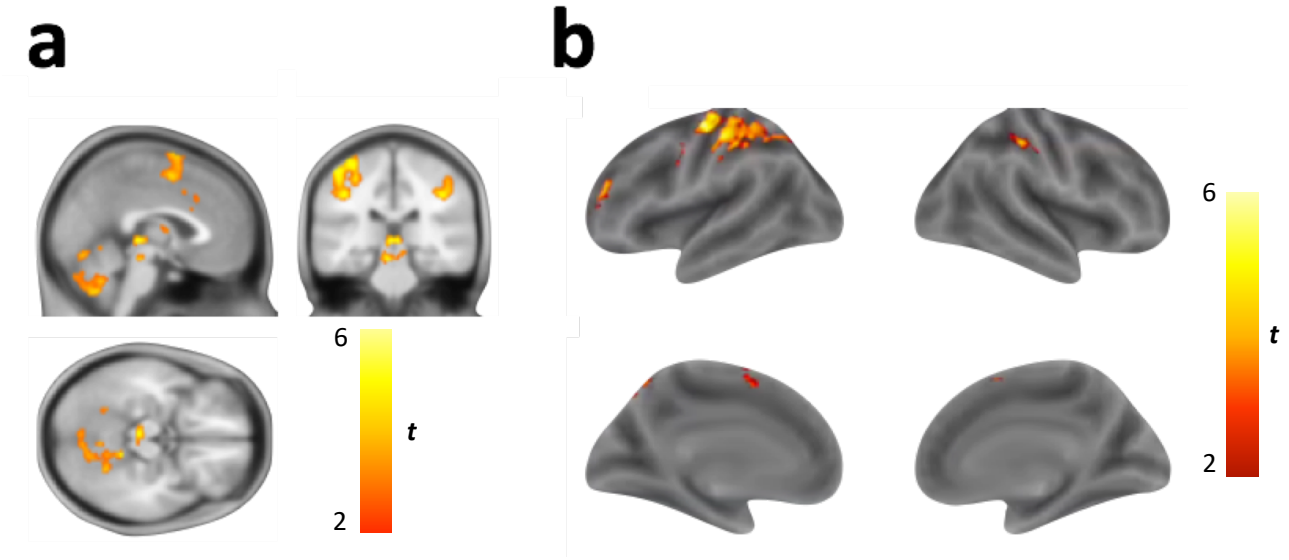

Brain regions showing significantly greater fMRI activation encoding Bayesian Surprise vs information theoretic Surprise (D_{KL} > I_S t-contrast). **(a):** Small volume correction indicates that bilateral regions of the SN/VTA and ventral striatum encode D_{KL} to a significantly greater extent than they encode I_S. SN/VTA peaks: (Right peak Montreal Neurological Institute (MNI) coordinates, 12 -26 -12, P_{peak} = 0.03, T_{peak} = 4.06, and left peak MNI, -9 -26 -14, P_{peak} = 0.03, T_{peak} = 4.03). Ventral striatum peaks (left peak MNI, -12 -15 -4, P_{peak} = 0.001, T_{peak} = 5.33, and right peak MNI, 8 15 -4, P_{peak} = 0.02, T_{peak} = 4.19). Image thresholded at P < 0.005 (unc.) cluster extent threshold > 100 for illustration purposes only. **(b):** Significant clusters displayed at family-wise error corrected $P_{cluster}$ < 0.05 (Voxel cut-off P<0.001 (unc.), critical cluster threshold = 244), projected onto inflated cortical surface. Significant clusters include left middle frontal gyrus, left supplementary motor cortex, and bilateral parietal cortex. Colour bar represents t-values.

Fig S2

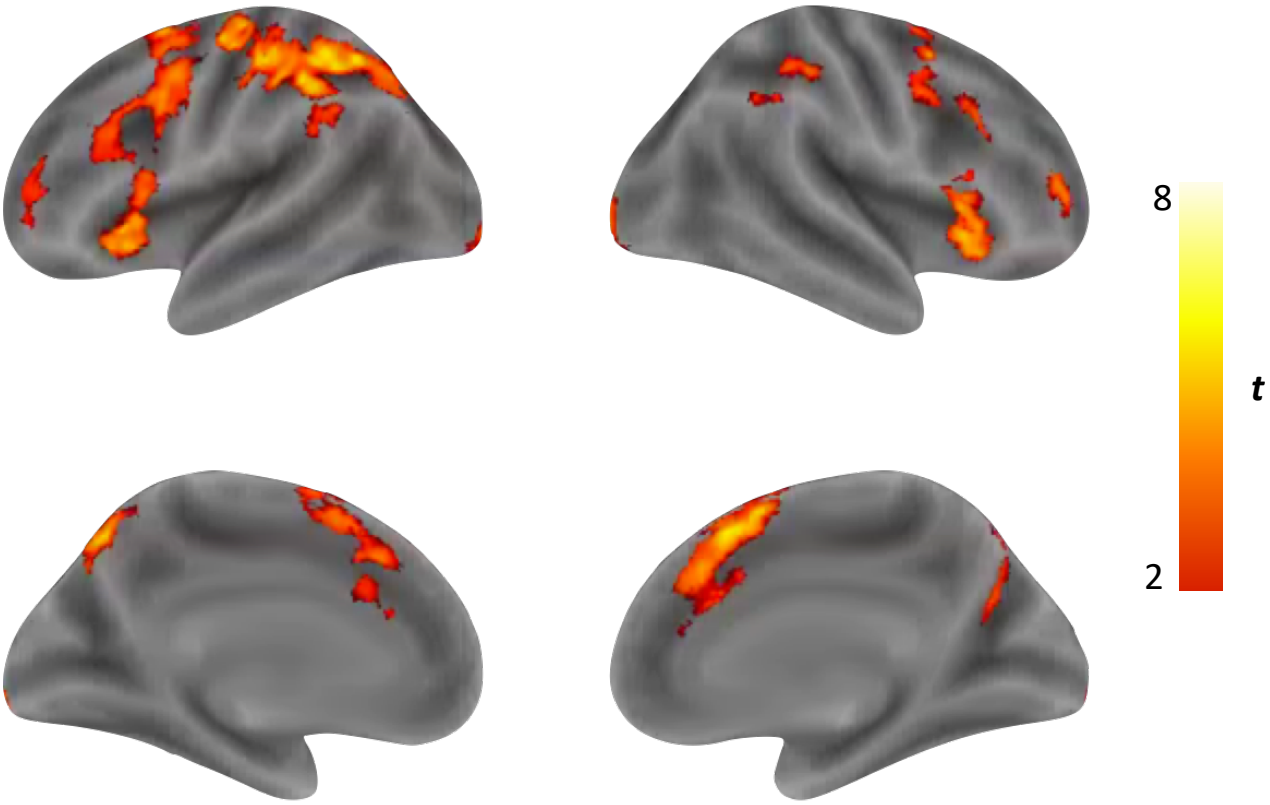

fMRI neural activity encoding Bayesian Surprise projected onto inflated cortical surface. Significant clusters of activation encoding Bayesian surprise across the whole brain displayed at family-wise error (FWE) corrected $P_{cluster} < 0.05$. (Voxel cut-off P < 0.001 (unc.), critical cluster threshold = 290), including posterior parietal cortex and lateral prefrontal cortex (see **SI Table S3** for details). Colour bar represents t-values.

Fig. S3

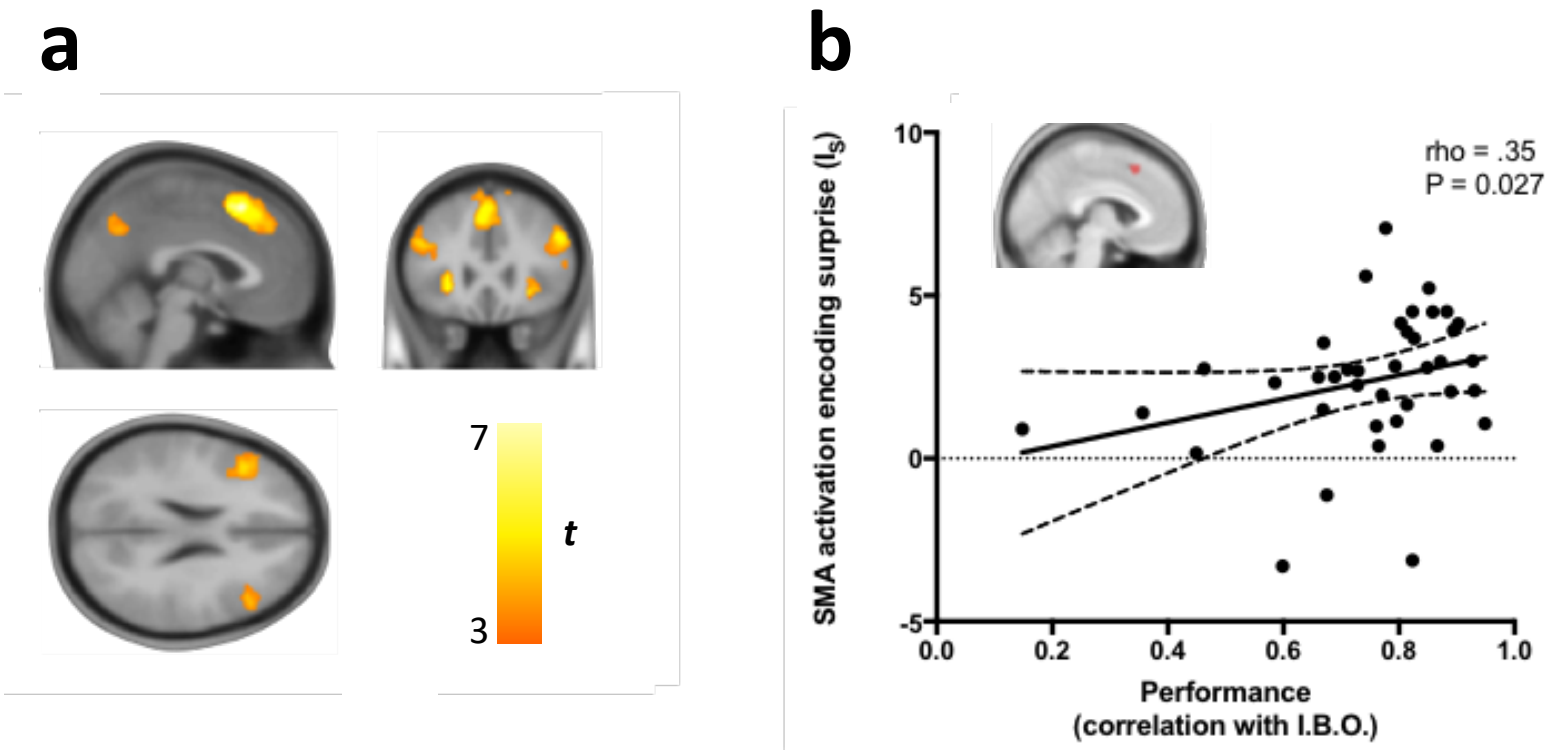

fMRI neural activity encoding information-theoretic surprise. (a) Clusters of activation encoding information-theoretic surprise across the whole brain, including the pre-supplementary motor area and left anterior insula. Image thresholded at P < 0.001 (unc.) with cluster extent threshold > 100 for illustration purposes only (see **SI Table S4** for family-wise error corrected cluster results). Colour bar represents t-values. **(b)** A cluster of voxels in the pre-supplementary motor area (shown in red) was significant at whole brain family-wise error (FWE) corrected $P_{peak} < 0.05$ level (peak Montreal Neurological Institute (MNI), -3 20 51, cluster size = 167, $P_{peak} = 0.001$, $T_{peak} = 7.72$). The effect size of this activation within this cluster (principle eigenvariate of parameter estimates for information-theoretic surprise contrast) positively correlated with participants' performance on the task (measured as the correlation between observed belief ratings and predictions of an ideal Bayesian observer (I.B.O.) model). Broken trendline represents 95% confidence bounds. SMA (pre-supplementary motor area).

Fig. S4

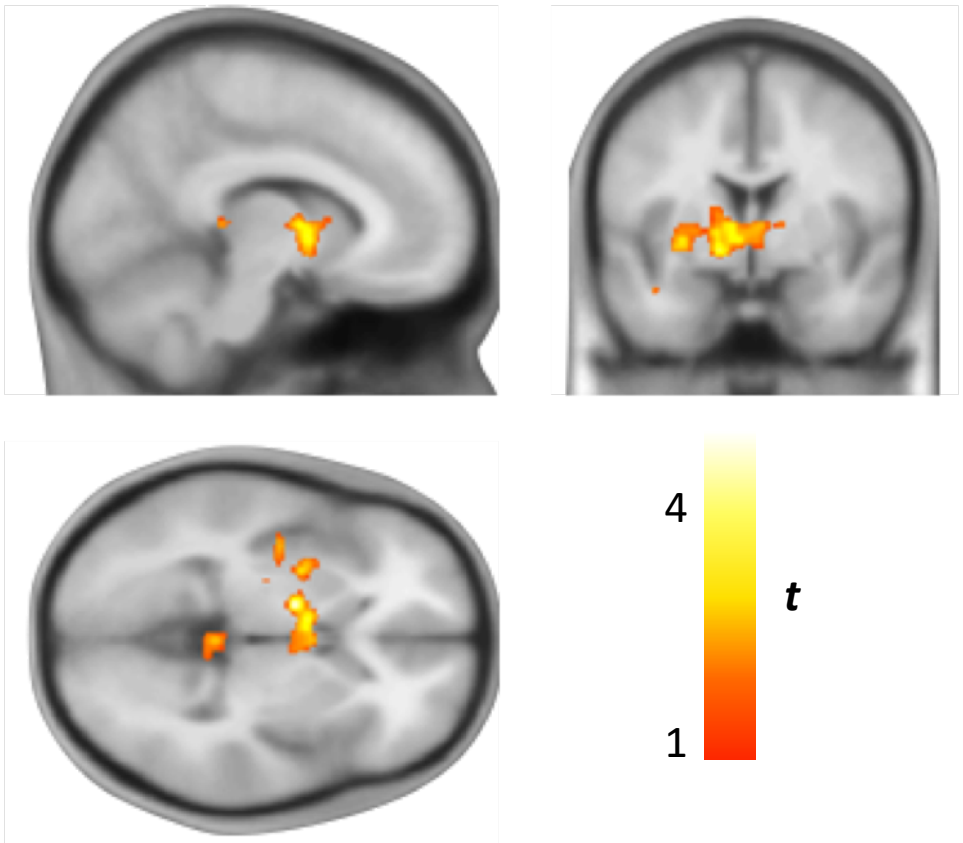

fMRI neural activity encoding signed reward prediction error. Clusters surviving whole brain family-wise error (FWE) correction at $P_{cluster} < 0.05$, applying a very liberal $P < 0.05$ (unc.) voxel-level cut-off. At this threshold there is a single large cluster of activation within the left striatum (peak Montreal Neurological Institute (MNI), -15 -3 -2, $P_{cluster} = 0.006$, $T_{peak} = 4.83$) surviving $P < 0.05$ corrected at whole brain level (critical cluster threshold = 4111). These results should be interpreted with caution given the very liberal cluster defining threshold used. Colour bar represents t-values.

Fig. S5

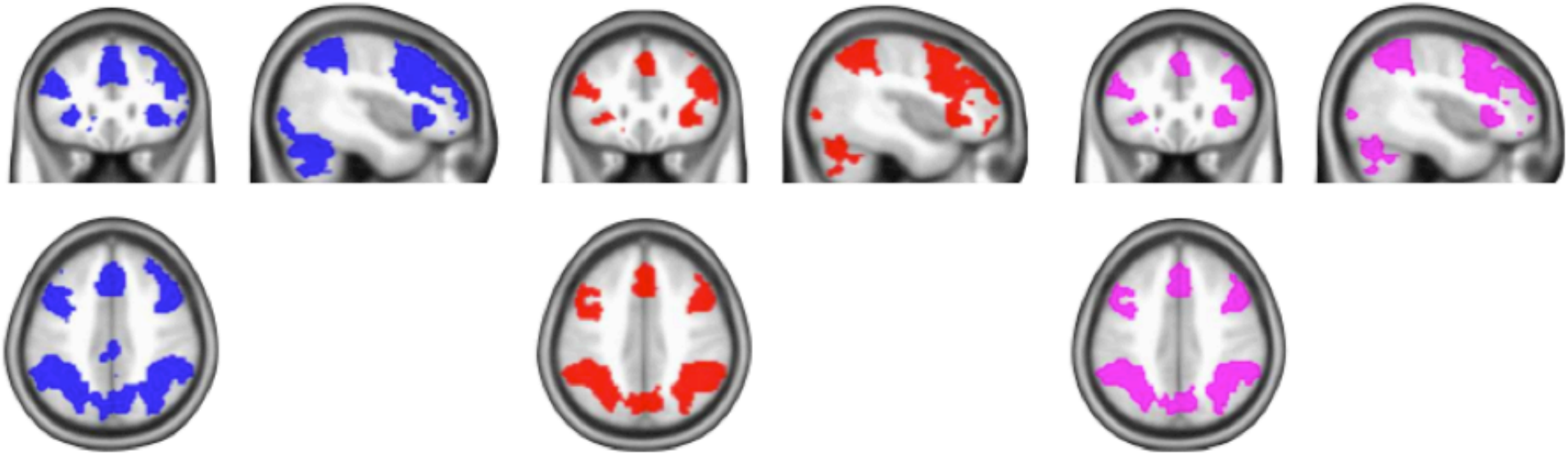

fMRI neural activity encoding uncertainty over prior beliefs at cue presentation.

Left: **Subjective uncertainty:** Blue clusters surviving whole brain family-wise error (FWE) correction at $P_{cluster} < 0.05$ from GLM1 (belief uncertainty at cue presentation defined as subjective uncertainty reported on rating bar on previous trial). See **SI Table S5** for details.

Middle: **Model-derived uncertainty:** Red clusters surviving whole brain FWE correction at $P_{cluster} < 0.05$ from GLM2 (belief uncertainty at cue presentation defined as entropy over model-derived prior belief distribution on the same trial). See **SI Table S5** for details.

Right: **Intersection:** Violet clusters representing the intersection of voxels surviving whole brain FWE correction at $P_{cluster} < 0.05$ in both GLM1 and GLM2.

Fig. S6

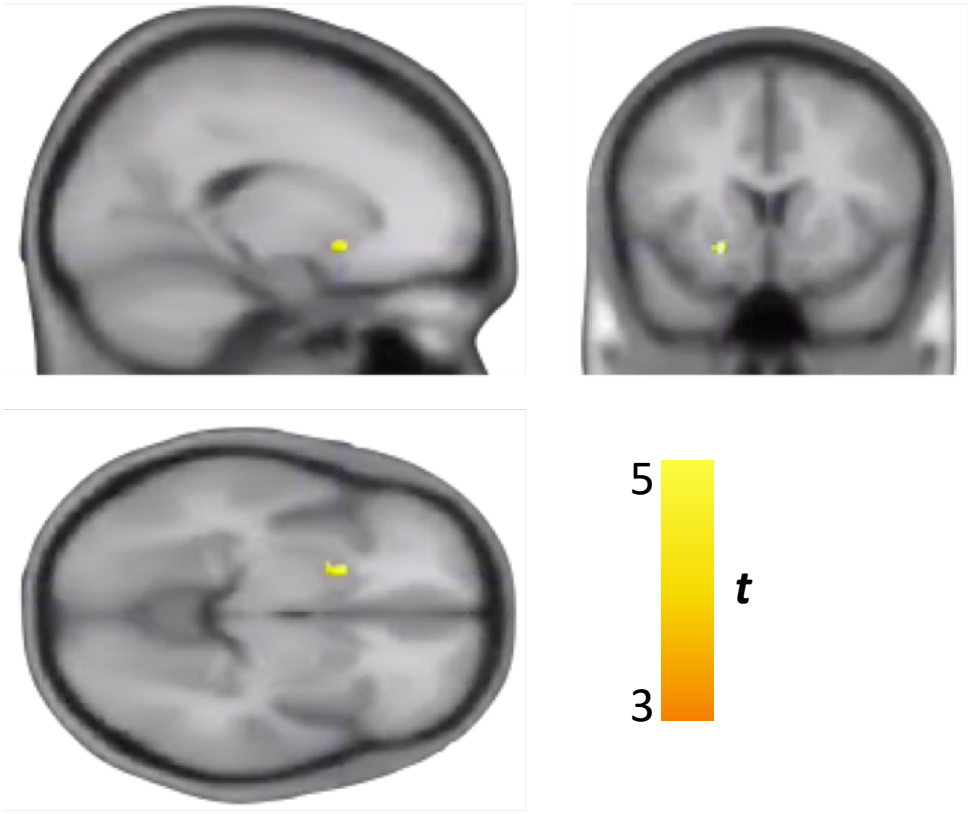

Whole brain analysis showing voxels where a participant's neural activation (1st level parameter estimate) encoding Bayesian surprise is predicted by the participant's whole striatum dopamine release capacity, with a negative linear relationship. This relationship is significant following small volume correction (within combined SN/VTA and ventral striatum ROI) in the left ventral striatum (peak Montreal Neurological Institute (MNI) coordinates, -20 15 -9, P_{peak} = 0.002, T_{peak} = 6.31). Image thresholded at $P < 0.001$ (unc.) with inclusive ROI mask, for illustration purposes. Colour bar represents t-values.

Fig. S7

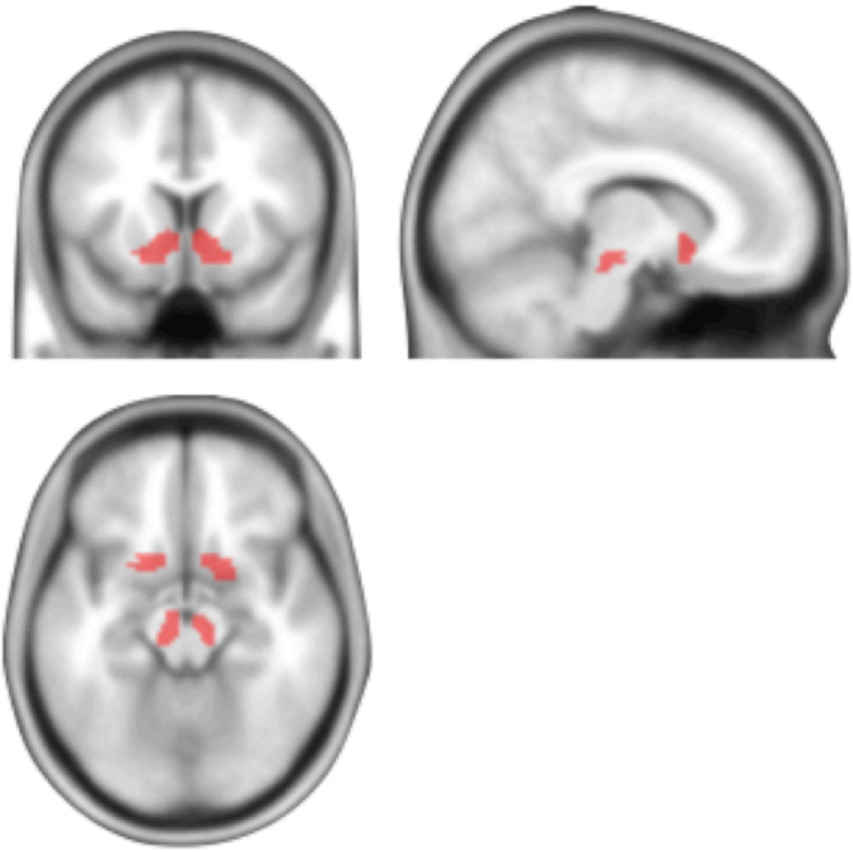

Combined substantia-nigra/ventral tegmental area (SN/VTA) and ventral striatum mask used for ROI analysis. Masks derived from [1,9].

Table S1

Mean individual parameter estimates of cue validity (ψ) and state transition probability (1-δ).

Participant	δ	ψ
1	0.83	0.96
2	0.98	0.95
3	0.94	0.76
4	0.93	0.81
5	0.94	0.86
6	0.97	0.97
7	0.91	0.98
8	0.97	0.98
9	0.93	0.93
10	0.97	0.89
11	0.97	0.99
12	0.90	0.76
13	0.96	0.97
14	0.91	0.71
15	0.96	0.96
16	0.92	0.89
17	0.99	0.93
18	0.94	0.88
19	0.94	0.96
20	0.95	0.96
21	0.82	0.96
22	0.93	0.97
23	0.50	0.89
24	0.95	0.91
25	0.89	0.90
26	0.88	0.65
27	0.90	0.63
28	0.91	0.84
29	0.85	0.95
30	0.93	0.93
31	0.95	0.83
32	0.83	1.00
33	0.93	0.83
34	0.97	0.94
35	0.97	0.99
36	0.98	0.84
37	0.91	1.00
38	0.89	0.97
39	0.93	0.95

Table S2

Results from the univariate (Model 1) and multivariate (Model 2) quadratic regression models, demonstrating an inverted-U relationship between striatal baseline D2/3R availability (BP_{ND}) and trial-by-trial behavioural sensitivity to meaningful information (mean belief shift on informative vs. non-informative trials). **Model 1:** $Behavioural\ sensitivity = \beta_0 + \beta_1 BP_{ND} + \beta_2 (BP_{ND})^2$, $F_{2,33}$ = 3.42, adjusted R^2 = .12, model *P* = 0.04. **Model 2:** $Behavioural\ sensitivity = \beta_0 + \beta_1 BP_{ND} + \beta_2\ Age + \beta_3\ BMI + \beta_4 (BP_{ND})^2$, $F_{4,31}$ = 3.40, adjusted R^2 = .22, model *P* = 0.02. Quadratic term has been mean-centred for both models. BMI = body mass index. $\mathrm{BP_{ND}}$ = [^{11}C]-(+)-PHNO non-displaceable binding potential within whole striatum region of interest.

	$\boldsymbol{\beta}$	Standard Error	*T* statistic	*P* value
Model 1				
Intercept	0.89	0.94	0.95	0.35
$\mathrm{BP_{ND}}$	0.50	0.44	1.13	0.26
$\mathrm{BP_{ND}}^2$	-3.21	1.47	-2.19	0.04
Model 2				
Intercept	0.33	1.72	0.19	0.85
$\mathrm{BP_{ND}}$	0.88	0.52	1.68	0.10
Age	0.04	0.02	1.81	0.08
BMI	-0.05	0.03	-1.70	0.10
$\mathrm{BP_{ND}}^2$	-4.07	1.49	-2.73	0.01

Table S3

Whole brain effects for Bayesian surprise (Kullback-Leibler divergence). Clusters of activation surviving whole brain family-wise error (FWE) corrected $P_{cluster}$ < 0.05 threshold (voxel cut-off P < 0.001 (unc.), critical cluster threshold = 290). Anatomical label and MNI co-ordinates are reported for the voxel with the maximum t-statistic from each cluster. MNI (Montreal Neurological Institute), dACC (dorsal anterior cingulate cortex), pre-SMA (pre-supplementary motor area).

					MNI coordinates (mm)		
Anatomical label	$P(FWE)_{cluster}$	**Cluster size**	T_{peak}	Z_{peak}	**x**	**y**	**z**
Left thalamus/brainstem	<0.001	1045	8.82	6.47	-3	-24	0
Left pre-SMA/dACC (cluster includes left supramarginal gyrus and right middle/superior frontal gyrus)	<0.001	31924	7.64	5.91	0	9	60
Left cerebellum	<0.001	1215	7.43	5.81	-38	-62	-28
Right cerebellum	<0.001	3450	6.3	5.18	36	-51	-32
Right cerebellum	<0.001	1630	5.63	4.77	30	-63	-46
Left occipital pole	0.008	382	5.6	4.75	-22	-102	-6
Right middle frontal gyrus	0.001	591	5.52	4.7	34	54	9
Right occipital pole	0.001	586	5.44	4.65	22	-102	-2
Right precuneus / superior parietal lobule	0.003	460	5.43	4.64	14	-66	42
Right supramarginal gyrus	0.005	420	4.91	4.3	42	-27	39
Right angular gyrus / supramarginal gyrus	0.029	290	4.91	4.29	48	-46	42
Left middle frontal gyrus	0.001	578	4.86	4.26	-33	45	8

Table S4

Whole brain effects for information-theoretic surprise. Clusters surviving whole brain family-wise error (FWE) corrected $P_{cluster} < 0.05$ threshold (voxel cut-off $P < 0.001$ (unc.), critical cluster threshold = 306). Anatomical label and MNI co-ordinates are reported for the voxel with the maximum t-statistic from each cluster. MNI (Montreal Neurological Institute), pre-SMA (pre-supplementary motor area).

Anatomical label					**MNI coordinates (mm)**		
	$P(FWE)_{cluster}$	**Cluster size**	T_{peak}	Z_{peak}	**x**	**y**	**z**
Left pre-SMA	<0.001	3441	7.72	5.95	-3	20	51
Left anterior insula and inferior frontal gyrus	0.016	310	5.92	4.95	-28	24	-3
Right middle frontal gyrus and inferior frontal gyrus	<0.001	1582	5.83	4.9	50	22	30
Left middle frontal gyrus	<0.001	1748	4.83	4.24	-48	21	34
Left angular gyrus and left superior parietal lobule	0.017	306	4.67	4.12	-32	-63	42
Precuneus (bilateral)	0.002	451	4.3	3.85	3	-64	34

Table S5

Whole brain effects for subjective belief uncertainty (GLM1) and model-derived belief uncertainty (entropy over prior beliefs) (GLM2) at cue onset. Clusters surviving whole brain family-wise error (FWE) corrected $P_{cluster} < 0.05$ threshold (voxel cut-off $P < 0.001$ (unc.), critical cluster threshold = 2343(GLM1) and 637(GLM2)). MNI co-ordinates are reported for the voxel with the maximum t-statistic from each cluster. MNI (Montreal Neurological Institute).

					MNI coordinates (mm)		
Anatomical label	$P(FWE)_{cluster}$	**Cluster size**	T_{peak}	Z_{peak}	**x**	**y**	**z**
GLM1 (subjective uncertainty)							
Bilateral frontal cortex (including dorsolateral prefrontal cortex and medial prefrontal cortex), anterior insula and subcortical structures (including striatum).	<0.001	49557	9.98	6.95	-20	16	10
Bilateral occipito-parietal cortex and cerebellum	<0.001	66515	9.57	6.79	-38	-72	-50
Middle and Posterior cingulate cortex	<0.001	2348	9.25	6.66	-4	-26	30
GLM2 (model-derived uncertainty)							
Bilateral occipito-parietal cortex and cerebellum	<0.001	42790	8.95	6.49	-10	-80	-34
Right anterior insula and dorsolateral prefrontal cortex	<0.001	11433	7.23	5.67	33	30	-3
Left anterior insula and dorsolateral prefrontal cortex	<0.001	9043	7.12	5.61	-27	24	-3
Medial prefrontal cortex (pre-supplementary motor area)	<0.001	2591	6.79	5.44	4	33	39
Subcortical nuclei, including thalamus and striatum	<0.001	2210	6.3	5.16	9	-6	9
Left middle frontal gyrus	<0.001	1198	6.09	5.03	-39	56	14
Posterior cingulate cortex	<0.001	1030	5.33	4.56	3	-36	27
Right middle and inferior temporal gyrus	<0.001	1054	5.2	4.48	58	-50	-14
Left middle and superior temporal gyrus	<0.001	637	4.43	3.94	-64	-40	3

Table S6

Mean pairwise correlations (Pearson's r) [and 95% C.I.] between parametric regressors at monetary outcome, used in the fMRI first-level general linear model (GLM).

	Information-theoretic surprise	**Reward prediction error**	**Money outcome**
Bayesian-surprise	.53 [.49, .58]	-.002 [-.03, .02]	-.002 [-.02, .02]
Information-theoretic surprise	1	.019 [-.02, .05]	.008 [-.01, .02]
Reward prediction error		1	.59 [.57, .61]

REFERENCES FOR SI APPENDIX

1. Schwartenbeck P, FitzGerald THB, Dolan R. Neural signals encoding shifts in beliefs. *Neuroimage* 2016;125:578-586.
2. Jack CR, Bernstein MA, Fox NC, Thompson P, Alexander G, Harvey D, Borowski B, Britson PJ, Whitwell JL, Ward C, Dale AM, Felmlee JP, Gunter JL, Hill DLG, Killiany R, Schuff N, Fox-bosetti S, Lin C, Studholme C, Decarli CS, Krueger G, Ward HA, Metzger GJ, Scott KT, Mallozzi R, Blezek D, Levy J, Debbins JP, Fleisher AS, Albert M, Green R, Bartzokis G, Glover G, Mugler J, Weiner MW, Study A. The Alzheimer ' s Disease Neuroimaging Initiative (ADNI): MRI Methods. *J. Magn. Reson. Imaging* 2008;27(4):685-691.
3. Kasper L, Bollmann S, Diaconescu AO, Hutton C, Heinzle J, Iglesias S, Hauser T, Sebold M, Manjaly Z-M, Pruessmann K, Stephan K. The PhysIO Toolbox for Modelling Physiological Noise in fMRI Data. *J. Neurosci. Methods* 2017;276:56–72.
4. Hutton C, Bork A, Josephs O, Deichmann R, Ashburner J, Turner R. Image Distortion Correction in fMRI: A Quantitative Evaluation. *Neuroimage* 2002;16(1):217-240.
5. Ashburner J. A fast diffeomorphic image registration algorithm. *Neuroimage* 2007;38(1):95-113.
6. Glover GH, Li T, Ress D. Image-Based Method for Retrospective Correction of Physiological Motion Effects in fMRI: RETROICOR. *Magn. Reson. Med.* 2000;44:162-167.
7. Hutton C, Josephs O, Stadler J, Featherstone E, Reid A, Speck O, Bernarding J, Weiskopf N. The impact of physiological noise correction on fMRI at 7T. *Neuroimage* 2011;57(1-4):101-112.
8. Harvey AK, Pattinson KTS, Brooks JCW, Mayhew SD, Jenkinson M, Wise RG. Brainstem functional magnetic resonance imaging: Disentangling signal from physiological noise. *J. Magn. Reson. Imaging* 2008;28(6):1337-1344.
9. Martinez D, Slifstein M, Broft A, Mawlawi O, Hwang D-R, Huang Y, Cooper T, Kegeles L, Zarahn E, Abi-Dargham A, Haber SN, Laruelle M. Imaging Human Mesolimbic Dopamine Transmission With Positron Emission Tomography. Part II: Amphetamine-Induced Dopamine Release in the Functional Subdivisions of the Striatum. *J. Cereb. Blood Flow Metab.* 2003;23(3):285-300.
10. Schwartenbeck P, FitzGerald THB, Mathys C, Dolan R, Friston K. The Dopaminergic Midbrain Encodes the Expected Certainty about Desired Outcomes. *Cereb. Cortex* 2015;25(10):3434-3445.
11. Gunn RN, Lammertsma AA, Hume SP, Cunningham VJ. Parametric Imaging of Ligand-Receptor Binding in PET Using a Simplified Reference Region Model. *Neuroimage* 1997;6(4):279-287.
12. Lammertsma AA, Hume SP. Simplified reference tissue model for PET receptor studies. *Neuroimage* 1996;4(3):153-158.
13. Tziortzi AC, Searle GE, Tzimopoulou S, Salinas C, Beaver JD, Jenkinson M, Laruelle M, Rabiner EA, Gunn RN. Imaging dopamine receptors in humans with [11C]-(+)-PHNO: Dissection of D3 signal and anatomy. *Neuroimage* 2011;54(1):264-277.
14. Cools R, D'Esposito M. Inverted-U-shaped dopamine actions on human working memory and cognitive control. *Biol. Psychiatry* 2011;69(12):e113-e125.
15. Cox SML, Frank MJ, Larcher K, Fellows LK, Clark CA, Leyton M, Dagher A. NeuroImage Striatal D1 and D2 signaling differentially predict learning from positive and negative outcomes. *Neuroimage* 2015;109:95-101.
16. Caravaggio F, Nakajima S, Borlido C, Remington G, Gerretsen P, Wilson A, Houle S, Menon M, Mamo D, Graff-Guerrero A. Estimating Endogenous Dopamine Levels at D2 and D3 Receptors in Humans using the Agonist Radiotracer [(11)C]-(+)-PHNO. *Neuropsychopharmacology* 2014;39(12):2769-76.